

## Adsorption of linear alkyl benzene sulfonates on oil–water interface: Effects of $\text{Na}^+$ , $\text{Mg}^{2+}$ and $\text{Ca}^{2+}$ ions



Svetoslav E. Anachkov<sup>a</sup>, Slavka Tcholakova<sup>a,\*</sup>, Dora T. Dimitrova<sup>a</sup>, Nikolai D. Denkov<sup>a</sup>, Narayanan Subrahmaniam<sup>b</sup>, Panchanan Bhunia<sup>b</sup>

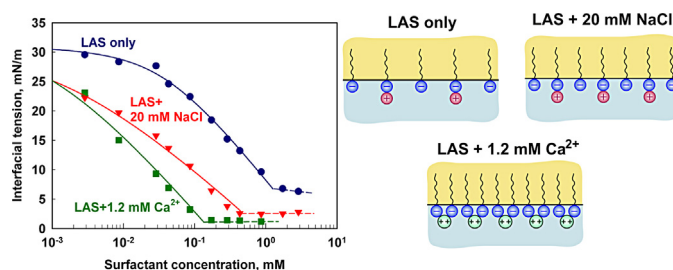
<sup>a</sup> Department of Chemical Engineering, Faculty of Chemistry and Pharmacy, Sofia University, Sofia 1164, Bulgaria

<sup>b</sup> Unilever R&D, 64 Main Road, Whitefield, Bangalore 560066, India

### HIGHLIGHTS

- Interfacial tension of LAS + 1.2 mM  $\text{Ca}^{2+}$  is much lower than LAS + 20 mM NaCl.
- This is due to a specific interaction between LAS and  $\text{Ca}^{2+}$  ions (3.5 kT).
- The interaction between LAS and  $\text{Na}^+$  is purely electrostatic.
- The area-per molecule on A–W interface is much smaller than that on O–W.
- Oil molecules intercalate in between the adsorbed surfactant molecules.

### GRAPHICAL ABSTRACT



### ARTICLE INFO

#### Article history:

Received 15 September 2014

Received in revised form 29 October 2014

Accepted 30 October 2014

Available online 7 November 2014

#### Keywords:

Linear alkyl benzene sulfonates

Adsorption

Fluid–fluid interfaces

Ionic binding effects

Hardness ions

### ABSTRACT

Linear alkyl benzene sulfonates (LAS) are among the most important industrial and house-hold surfactants. Here we study the LAS adsorption properties at oil–water interface in the presence of divalent counter-ions ( $\text{Mg}^{2+}$  and  $\text{Ca}^{2+}$ ). Interfacial tension data are obtained and interpreted using a detailed thermodynamic model for surfactant adsorption, which explicitly accounts for counter-ion binding (Kralchevsky et al. Langmuir 15 (1999) 2351). The obtained results show that the hardness ions (i) reduce very significantly the area-per-molecule in the adsorption layer; (ii) reduce strongly the magnitude of the negative surface potential, neutralizing almost completely the adsorbed LAS molecules; (iii) bind strongly to the adsorption layer via both electrostatic attraction and specific attraction of magnitude around 3.5 kT. The limiting area-per-molecule at oil–water interface is shown to be significantly larger than the respective area at air–water interface. The latter result indicates that the oil molecules are able to intercalate in between the surfactant molecules in the adsorption layer and, thus, to disrupt the molecular packing at the oil–water interface.

© 2014 Elsevier B.V. All rights reserved.

## 1. Introduction

Surfactants are widely used as emulsifiers, foamers, detergents, solubilizers and wetting agents in many pharmaceutical, personal care, home care and food products. Linear alkyl benzene sulfonates

(LAS) are among the most important anionic surfactants, because they are irreplaceable in several important applications, most noticeably in detergency and laundry.

To better understand their physico-chemical properties at air–water interface and in bulk solution, various LAS isomers and their mixtures have been synthesized and extensively studied through the years [1–9]. Meader and Criddle [1] employed the Langmuir trough method to determine the cross-sectional areas in adsorption layers of different positional isomers of dodecyl

\* Corresponding author. Tel.: +359 888246961.

E-mail addresses: [sc@cpce.uni-sofia.bg](mailto:sc@cpce.uni-sofia.bg), [sc@dce.uni-sofia.bg](mailto:sc@dce.uni-sofia.bg) (S. Tcholakova).

benzene sulfonates. To circumvent the issues related to surfactant solubility in the aqueous sub-phase, these authors used 95% saturated sodium nitrate solution as a substrate in their measurements. LAS positional isomers were thoroughly studied also by Ma et al. [2] in terms of LAS solubility, self-assembly, and air–water interfacial activity. The interfacial activity and the properties of the adsorption layers were investigated by surface tension measurements, followed by theoretical interpretation using Gibbs adsorption isotherm.

By applying neutron reflectivity (NR) and small-angle neutron scattering (SANS), Tucker et al. [3,4] focused on surface and phase behavior of LAS isomers in presence and in absence of calcium counter-ions. They found that calcium interacts strongly with LAS headgroups, which leads to complexation in solution and to multilayer formation at the air–water interface. In contrast, such effects were not observed when simple monovalent counter-ions were studied.

LAS behavior at oil–water interfaces yet remains less understood. Apart from a dissipative particle dynamics (DPD) study [5] and a comparison of experimental results with computations [6], there are almost no papers in the literature for LAS adsorption on oil–water interfaces, especially in the presence of divalent cations, such as  $Mg^{2+}$  and  $Ca^{2+}$ . Probably, this is to be expected, because only a few experimental techniques, such as nonlinear vibrational sum-frequency spectroscopy [10], second harmonic generation [11], ellipsometry [12,13] and specular neutron reflectivity [14], can be applied for the direct investigation of liquid–liquid interfaces. These techniques are very difficult and time-consuming. Therefore, one of the primary methods to study LAS interfacial behavior continues to be the data interpretation from interfacial tension measurements.

The main purpose of our current study is to acquire deeper quantitative understanding of the main factors and forces, which govern LAS adsorption on oil–water interface. Furthermore, we are specifically interested in the effects of  $Mg^{2+}$  and  $Ca^{2+}$  on LAS adsorption. To accomplish our goals, we measure the interfacial tension isotherms and interpret them with a detailed theoretical model, which accounts for the counter-ion binding and provides information about the important molecular properties, such as area-per molecule, free energy for surfactant adsorption and binding energies of counter-ions to LAS adsorption layers.

To determine the specific patterns of LAS adsorption on oil–water interface, we compare results for both oil–water and air–water interfaces. As noted by various authors, the effect of the non-polar phase on the properties of the surfactant adsorption layers could be rather significant. Two mechanisms are proposed to explain the observed differences between air–water and oil–water interfaces: (i) direct intercalation of the oil molecules in between the adsorbed surfactant molecules or (ii) partial dissolution of the surfactant molecules in the oily phase. Irrespective of the operable mechanism, the outcome is a decreased surfactant adsorption and reduced cohesion between the adsorbed molecules in the case of oil–water interface, as compared to air–water interface [15].

The article is organized as follows: Section 2 provides information about the materials and methods used. Section 3 presents the thermodynamic model used for interpretation of the interfacial tension data. The numerical algorithm for data processing is described in Section 4. The experimental and numerical results on LAS adsorption are presented and discussed in Section 5. Section 6 summarizes the main conclusions.

## 2. Materials and methods

### 2.1. Materials

We studied the anionic surfactant linear alkyl benzene sulfonate, sodium salt (technical grade, ca. 92%, donated by Unilever

R&D), for which sodium dodecyl benzene sulfonate is the primary component. As oil phase we used commercial soy bean oil (SBO) which was purified from polar contaminants by passing it through a column filled with activated magnesium silicate (Florisil®, Sigma–Aldrich, Germany). Multiple passes were performed until the equilibrium interfacial tension against pure water became  $30.5 \pm 0.5$  mN/m [16–18].

All solutions were prepared with deionized water which was purified by an Elix 3 water purification system (Millipore). For preparation of the salt solutions we used NaCl,  $CaCl_2 \cdot 6H_2O$  and  $MgCl_2 \cdot 6H_2O$ , all products of Sigma–Aldrich, Germany.

### 2.2. Interfacial tension measurements

The interfacial tension of the surfactant solutions against soy bean oil (SBO), in presence and in absence of electrolytes, was measured by applying the axisymmetric drop shape analysis (DSA) to pendant oil drops in aqueous surfactant solution. The measurements were conducted on DSA 100 instrument (Krüss GmbH, Germany), at  $T=25^\circ C$ , using a specially designed thermostating chamber (model TC40, Krüss GmbH, Germany). The obtained dependences for the dynamic surface tension  $\sigma(t)$  were converted to  $\sigma(t^{-1/2})$  and fitted with linear regression. From the extrapolation of this fit to infinite times, the equilibrium value of the interfacial tension was determined and used to construct the adsorption isotherms  $\sigma(c_{1\infty})$ , where  $c_{1\infty}$  is the surfactant concentration in the bulk aqueous phase (for the notation, see Section 3).

### 2.3. Surface tension measurements

Wilhelmy plate method [19,20] was used to estimate the equilibrium surface tension of the surfactant solutions. The measurements were performed on a tensiometer K100 (Krüss GmbH, Germany) using a platinum plate. Before each measurement, the plate was rinsed with ethanol and deionized water, followed by heating in a flame to remove any residual organic contaminants. The typical measuring accuracy of the method is  $\pm 0.1$  mN/m. All measurements were performed at  $25.0 \pm 0.5^\circ C$ .

### 2.4. Zeta potential measurements of oil droplets

We conducted zeta potential measurements of oil droplets to determine the surface electric potential of LAS interfacial layer in the presence of electrolytes. The oil droplets consisted of purified SBO and the aqueous phase was the respective surfactant–electrolyte solution. Diluted oil-in-water emulsions, which contained less than 1 vol.% oil drops, were prepared by a rotor–stator homogenizer Ultra Turrax T25 (Janke & Kunkel GmbH, Germany), operating at 24,000 rpm. The duration of stirring was ca. 2 min for each emulsion.

The electrophoretic mobility experiments were performed on a Zetasizer Nano ZS device (Malvern, UK) using disposable zeta cells. The studied emulsions were thermostated in the zeta cell at  $25.0^\circ C$  for 120 s, before each series of 3 measurements. Several independent experiments were carried out for each system to check for reproducibility and the data scattering was always within the experimental error ( $\pm 5$  mV).

## 3. Theoretical model of ionic surfactant adsorption

### 3.1. Basic thermodynamics equations

Here we summarize the theoretical equations which describe ionic surfactant adsorption in the presence of electrolytes, according to the approach developed by Kralchevsky et al. [21] which considers explicitly the adsorption of counter-ions in both Stern

layer and diffuse electric layer at the interface. It should be noted that despite being a superior thermodynamical model, only few studies have employed this approach to study the adsorption behavior of ionic surfactants [21–23].

We consider solution of sodium alkyl benzene sulfonate LAS, in the presence of electrolytes NaCl and/or CaCl<sub>2</sub> or MgCl<sub>2</sub>. We denote the various species with the following indices: 1 stands for the surface active ions (LAS), 2 for the counter-ions (Na<sup>+</sup>), 3 for the co-ions (Cl<sup>-</sup>) and 4 for the divalent counter-ions (Ca<sup>2+</sup> or Mg<sup>2+</sup>). The type of ionic surfactant determines the sign of the surface electric charge and potential  $\phi_s$ . For our system, LAS ions are negatively charged and so is the interface. The surface potential is expressed in dimensionless form as follows:

$$\Phi_s \equiv \frac{Z_1 e \phi_s}{kT}, \quad (1)$$

where  $Z_1$  is the charge of the surface active ion (in our case  $Z_1 = -1$  for LAS) and  $kT$  is the thermal energy. The dimensionless surface potential  $\Phi_s$  defined by Eq. (1) has positive values, irrespectively of the type of ionic surfactant. In terms of  $\Phi_s$  and assuming that the ions obey Boltzmann distribution, the subsurface concentrations of the various species,  $c_{is}$ , are given by:

$$c_{is} = c_{i\infty} \exp(-z_i \Phi_s), \quad z_i = \frac{Z_i}{Z_1} \quad (2)$$

where  $c_{i\infty}$  is the bulk concentration of these species far from the interface ( $i = 1, 2, 3, 4$ ). In our particular system:

$$z_1 = -z_2 = z_3 = 1, \quad z_4 = -2 \quad (3)$$

From physical viewpoint, it is reasonable to assume that the co-ions (Cl<sup>-</sup>) do not adsorb directly on the interface, viz.  $\Gamma_3 = 0$ , due to their strong electrostatic repulsion from the interface. On the other hand, the adsorption of counter-ions is nonzero and can be described by Stern adsorption isotherm [21]:

$$\frac{\Gamma_i}{\Gamma_1} = \frac{K_i c_{is}}{K_1 + K_2 c_{2s} + K_4 c_{4s}} \quad (i = 2, 4) \quad (4)$$

where  $\Gamma_2$  is the counter-ion adsorption for Na<sup>+</sup> and  $\Gamma_4$  stands for the adsorption of either Ca<sup>2+</sup> or Mg<sup>2+</sup>;  $K_1$ ,  $K_2$  and  $K_4$  are the respective adsorption constants. The surfactant adsorption  $\Gamma_1$  can be expressed by Volmer adsorption isotherm, which accounts for non-localized adsorption on the fluid–fluid interfaces, with no lateral interactions between the surfactant hydrocarbon tails [21]:

$$Kc_{1s} = \frac{\Gamma_1}{\Gamma_\infty - \Gamma_1} \exp\left(\frac{\Gamma_1}{\Gamma_\infty - \Gamma_1}\right) \quad (5)$$

here  $\Gamma_\infty$  denotes the maximum possible value of  $\Gamma_1$ . The value of  $\alpha_\infty = 1/\Gamma_\infty$  expresses the excluded area per surfactant molecule in the adsorption layer. The adsorption parameter  $K$  in Eq. (5) is related to the constants  $K_1$ ,  $K_2$  and  $K_4$  by the condition for thermodynamic compatibility of the surfactant adsorption isotherm with the counter-ion binding isotherm (see [21] for detailed explanations). This condition is fulfilled as long as:

$$K = K_1 + K_2 c_{2s} + K_4 c_{4s} \quad (6)$$

To formulate a complete set of equations, we also need a relationship that connects the surface charge density to the surface potential. Such a relation is given by Gouy equation which for our system reads [21]:

$$\Gamma_1 - \Gamma_2 - 2\Gamma_4 = \frac{2}{\kappa_c y} \sqrt{I_1 (y^2 - 1)} g_1, \quad (7)$$

where

$$I_1 \equiv c_{2\infty} + 3c_{4\infty}, \quad \lambda^2 \equiv \frac{c_{4\infty}}{I_1}, \quad y = \exp\left(\frac{\Phi_s}{2}\right), \quad (8)$$

$$g_1 = (1 - \lambda^2 + \lambda^2 y^2)^{1/2}$$

$I_1$  is the ionic strength of the solution and  $\kappa_c^2 \equiv 2e^2/\epsilon\epsilon_0 kT$ .

Finally, the interfacial tension,  $\sigma$ , and the related surface pressure,  $\pi = \sigma_0 - \sigma$ , is expressed in the form [21]:

$$\frac{\pi}{kT} \equiv \frac{\sigma_0 - \sigma}{kT} = J + 2F \quad (9)$$

where  $\sigma_0$  is the interfacial tension of the bare interface (without any surfactant adsorbed),  $J$  corresponds to Volmer adsorption isotherm of the surfactant, and  $2F$  is the electric term, which accounts for the contribution of the diffuse part of the electric double layer to the interfacial tension. The expression for  $J$  reads [21]:

$$J = \frac{\Gamma_\infty \Gamma_1}{\Gamma_\infty - \Gamma_1} \quad (10)$$

and the equation for  $F$  is [21]:

$$F = \begin{cases} \frac{\sqrt{I_1}}{\kappa_c} \left[ \left( y + \frac{2}{y} \right) g_1 - 3 + \frac{1 - 3\lambda^2}{\lambda} \ln \left| \frac{\lambda y + g_1}{\lambda + 1} \right| \right], & \lambda \neq 0 \\ \frac{2\sqrt{I_1}}{\kappa_c} \frac{(y - 1)^2}{y}, & \lambda = 0 \end{cases} \quad (11)$$

The case  $\lambda = 0$  corresponds to no additional 2:1 electrolyte in the surfactant solution ( $c_{4\infty} = 0$ ) and the expression for  $F$  is simplified by taking the limit  $\lambda \rightarrow 0$  in this case.

### 3.2. Adsorption parameters

Once the adsorption parameters are extracted from the interpretation of the interfacial tension data (see Section 4 for the respective numerical procedure), one can determine various molecular characteristics which provide valuable information for the adsorption layer and adsorption energies. For instance, the maximum adsorption  $\Gamma_\infty$  is directly related to the excluded area per molecule  $\alpha_\infty = 1/\Gamma_\infty$ . The parameter  $K_1$  gives the standard free energy of surfactant adsorption  $\Delta\mu_1^0$  from the solution to monolayer through the expression [21]:

$$K_1 = \frac{\delta_1}{\Gamma_\infty} \exp\left(\frac{\Delta\mu_1^0}{kT}\right) \quad (12)$$

where  $\delta_1$  is the thickness of the adsorption monolayer, which is approximately 2 nm for LAS [3,4]. An analogous equation holds for the counter-ion adsorption parameter (Stern constant) [21]:

$$\frac{K_i}{K_1} = \frac{\delta_i}{\Gamma_\infty} \exp\left(\frac{\Delta\mu_i^0}{kT}\right), \quad (i = 2, 4) \quad (13)$$

where  $\delta_i$  is the thickness of the Stern layer, which coincides with the diameter of a hydrated counter-ion and  $\Delta\mu_i^0$  is the standard free energy of counter-ion binding from the solution to the Stern layer. In our particular case, the Stern layer thicknesses are used as follows:  $\delta_2 = 0.36$  nm for Na<sup>+</sup>,  $\delta_4 = 0.41$  nm for Ca<sup>2+</sup> and  $\delta_4 = 0.43$  nm for Mg<sup>2+</sup> [24].

## 4. Numerical procedure

Below we explain how the above equations are used to fit the experimental data and to obtain the adsorption parameters:

- (1) The input data are the experimental set of values for the interfacial tension  $\sigma^{\text{exp}}(c_{1\infty}, c_{2\infty}, c_{4\infty})$ . Since the interfacial tension for pure fluids  $\sigma_0$  is known ( $\sigma_0 = 31$  mN/m for SBO/water and  $\sigma_0 = 72$  mN/m for air/water interface at 25 °C), one uses the surface pressure,  $\pi$ , instead of interfacial tension in the numerical calculations.  $\pi$  is a more convenient physical quantity when we compare air–water and oil–water interfaces.
- (2) We assign tentative values for  $K_1$ ,  $K_2$ ,  $K_4$  and  $\Gamma_\infty$ , which are to be determined as adjustable parameters from the best fit to the

experimental data. It is important to stress here that the fit is not very sensitive to the ratios  $K_2/K_1$  and  $K_4/K_1$ ; hence, these ratios were chosen from a list of discrete values.

- (3) To determine the dimensionless surface potential  $\Phi_s$ , we apply the bisection method. The starting interval  $0 < \Phi_s < 15$  is usually appropriate. To better specify the upper boundary of the interval for  $\Phi_s$ , the following two inequalities must hold:

(a) In the case of  $c_{4\infty} \neq 0$ ,  $\Phi_s$  should not exceed the boundary:

$$\Phi_s < -\frac{1}{2} \ln \left( \frac{K_4}{K_1} c_{4\infty} \right). \quad (14)$$

This condition ensures that  $\Gamma_1$  is positive (as required from physical viewpoint) and no charge reversal occurs as a result of counter-ion adsorption.

(b) The surfactant adsorption  $\Gamma_1$  can be obtained in the form  $\Gamma_1(\Phi_s)$  by substituting Eq. (4) for  $\Gamma_2$  and  $\Gamma_4$  into Eq. (7). Since  $\Gamma_1$  cannot exceed the maximum adsorption  $\Gamma_\infty$ ,  $\Phi_s$  is limited by the following inequality:

$$\Gamma_1(\Phi_s) < \Gamma_\infty \quad (15)$$

- (4) We substitute  $\Gamma_1(\Phi_s)$  into Eq. (5), which then becomes an implicit equation for  $\Phi_s$ . The latter is solved numerically.  
 (5) The theoretical running values of the interfacial tension  $\sigma^{th}$  ( $c_{1\infty}, c_{2\infty}, c_{4\infty}; K_1, K_2, K_4, \Gamma_\infty$ ) are calculated from Eqs. (9)–(11).  
 (6) The adjustable parameters  $K_1, K_2, K_4, \Gamma_\infty$  are determined by means of the least-squares method, viz. by numerical minimization of the merit function, defined as:

$$\chi(K_1, K_2, K_4, \Gamma_\infty) = \left\{ \frac{1}{N} \sum_{k=1}^N \left[ \sigma^{\exp}(c_{1\infty}^{(k)}, c_{2\infty}^{(k)}, c_{4\infty}^{(k)}) - \sigma^{th}(c_{1\infty}^{(k)}, c_{2\infty}^{(k)}, c_{4\infty}^{(k)}; K_1, K_2, K_4, \Gamma_\infty) \right]^2 \right\}^{1/2} \quad (16)$$

where we assumed that all experimental points have equal errors.  $N$  is the total number of the experimental values included in the fit.

The minimization algorithm used in step 6 of the numerical procedure is very straightforward. First, relative steps for the model parameters  $K_1$  and  $\Gamma_\infty$  are defined. For fixed  $K_2/K_1$  and  $K_4/K_1$ , starting from a given point  $(K_1, \Gamma_\infty)$ , a  $3 \times 3$  grid is constructed around it and the values of the merit function are calculated. Then all 9 values are compared, the initial guess is changed with the position where  $\chi$  is minimal, and the procedure is repeated again [25]. When the initial guess coincides with the local minimum for  $\chi$  on the grid, the relative steps are reduced twice. The algorithm stops when the relative steps become smaller than the chosen numerical precision. Finally, the position of the global minimum of the merit function  $\chi_{\min}$  is determined.

## 5. Results and discussion

### 5.1. Interfacial tension isotherms of LAS on oil–water interface

Our goal is to characterize the interfacial properties of LAS in the presence of sodium and hardness ions ( $\text{Mg}^{2+}$  or  $\text{Ca}^{2+}$ ). Therefore, we measured the interfacial tension  $\sigma(t)$  of surfactant solutions against soybean oil (SBO) using the pendant drop method. The adsorption isotherms of LAS in presence of  $\text{Na}^+$ ,  $\text{Mg}^{2+}$  and  $\text{Ca}^{2+}$  were constructed, as shown in Fig. 1. The isotherms exhibit a sharp transition in the slope at CMC. No minimum was observed in any of the measured isotherms, which is an evidence for high surfactant purity.

Fig. 1 shows that the addition of electrolyte lowers significantly the equilibrium interfacial tension; for example,  $\sigma$  at CMC is ca. 6 mN/m in absence of electrolyte, whereas,  $\sigma$  is 2.5 mN/m in the

presence of 50 mM NaCl (Fig. 1A). Similarly, hardness ions significantly affect surfactant adsorption, thus leading to very low interfacial tensions, even below 1 mN/m (Fig. 1B and C).

By comparing LAS isotherms in presence of  $\text{Na}^+$  and hardness ions (Fig. 2), we see that the effect of 20 mM NaCl on  $\sigma$  is smaller than the effect of 1.2 mM  $\text{Mg}^{2+}$  or 1.2 mM  $\text{Ca}^{2+}$ . In addition, one can notice that  $\text{Mg}^{2+}$  and  $\text{Ca}^{2+}$  ions have very similar effects on LAS interfacial tension in the concentration range studied (up to 1.2 mM).

The presence of electrolytes affects the critical micelle concentration (CMC) as well. The CMC of LAS without added electrolyte is 1.42 mM (Fig. 1A) which is in a good agreement with the literature values, reported to be in the range 1.0–2.6 mM [2,6–9]. As illustrated in Fig. S1A in the Supplementary Materials section, the CMC decreases upon addition of salt: from 1.42 mM (no added salt) to 0.20 mM (50 mM NaCl). The dependence of CMC on counter-ion concentration resembles a straight line in double log scale, thus following the Corrin–Harkins empirical relation [26].

The comparison of the data shown in Figs. S1A and S1B shows that only 0.6 mM  $\text{Ca}^{2+}$  is sufficient to reduce CMC nearly 10 times (from 1.42 mM to 0.15 mM). Tucker and co-workers [3] reported that the CMC of LAS in presence of 1 mM  $\text{CaCl}_2$  is ca. 0.3 mM, which is 2–3 times higher than the value expected from Fig. S1B. This difference is most probably due to the different source of LAS used in the two studies. The main conclusion, however, is the same – the divalent counter-ions, such as  $\text{Ca}^{2+}$ , bind very strongly to LAS and, therefore, reduce CMC very efficiently. On the contrary, monovalent cations, such as  $\text{Na}^+$ , have comparable effect at much higher concentrations only. Similar conclusion was reported also

for the cationic surfactant di-hexadecyl dimethyl ammonium bromide solutions at the air–water interface [27].

To gain deeper understanding of the influence of  $\text{Ca}^{2+}$  and  $\text{Mg}^{2+}$  ions on LAS adsorption on SBO–water interface, we conducted interfacial tension measurements, in which we kept the concentration of  $\text{Ca}^{2+}$  constant and varied the ionic strength by addition of NaCl. The obtained results are shown in Fig. 3. One sees that  $\sigma$  depends very weakly on the NaCl concentration in the presence of 1.2 mM  $\text{Ca}^{2+}$  ions. This is another illustration of the strong binding affinity of  $\text{Ca}^{2+}$  ions to LAS – the  $\text{Na}^+$  ions are unable to displace them.

### 5.2. Adsorption of LAS on oil–water interface

The interfacial tension isotherms were interpreted numerically, as explained in section 4. Having once determined the fit parameters  $K_1, K_2, K_4$  and  $\Gamma_\infty$  (see Table 1), one can compute not only the interfacial tension  $\sigma$ , but also: (i) surfactant adsorption,  $\Gamma_1$ ; (ii) surface coverage,  $\theta_s \equiv \theta_1 = \Gamma_1/\Gamma_\infty$ ; (iii) counter-ion adsorption (binding) in the Stern layer,  $\Gamma_2$  and  $\Gamma_4$ ; (iv) occupancy of the Stern layer by bound counter-ions,  $\theta_{\text{Na}} \equiv \theta_2 = \Gamma_2/\Gamma_1$  and  $\theta_{\text{Ca}} \equiv \theta_4 = \Gamma_4/\Gamma_1$ . Additionally, we can determine the dimensionless surface potential  $\Phi_s$ . Each of these properties can be evaluated for a given surfactant and salt concentrations, below the CMC.

First we present the numerical results for the surfactant surface coverage  $\theta_s$ , as a function of the surfactant concentration, see Fig. 4. When salt is added to the solution, the surfactant adsorption significantly increases, because the electrostatic repulsion between the surfactant headgroups on the interface is markedly screened. Interestingly, the surface coverage by the surfactant molecules,  $\theta_s$ ,

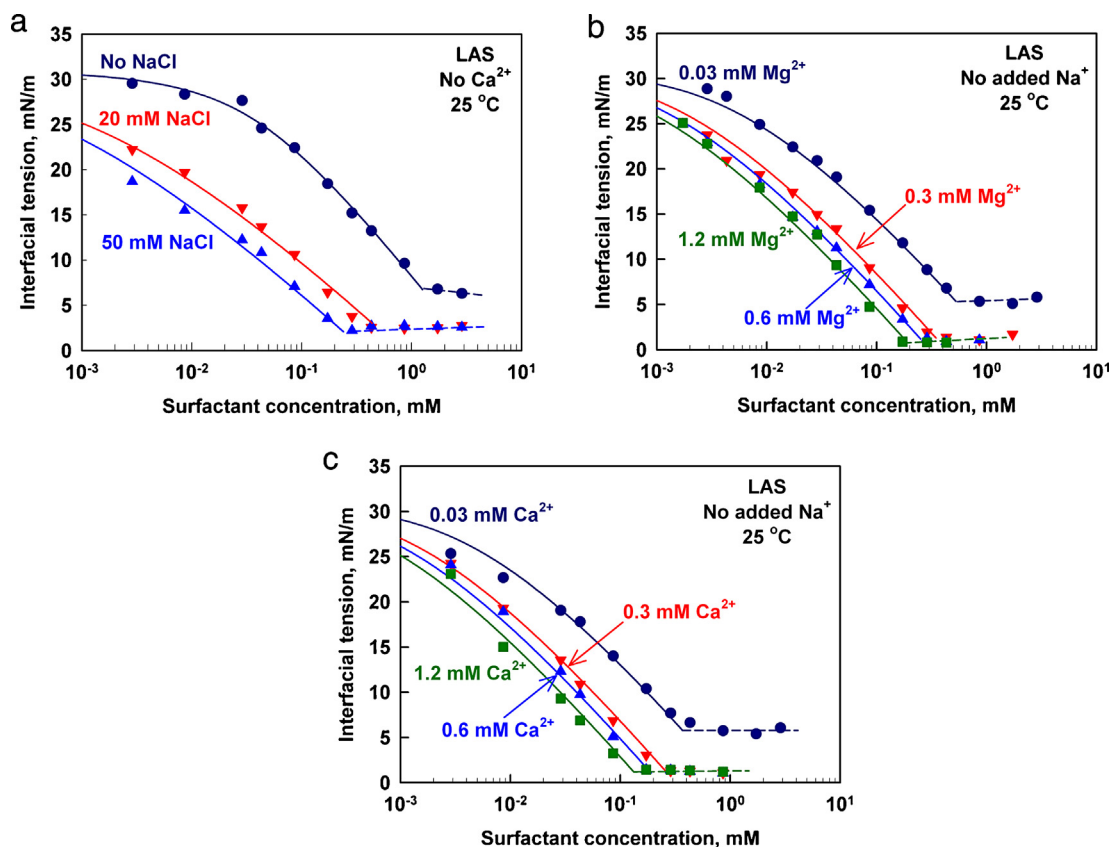


**Fig. 1.** Interfacial tension isotherms for LAS on SBO–water interface at various salt concentrations. The used salts are: (A) NaCl, (B)  $\text{MgCl}_2$  and (C)  $\text{CaCl}_2$ . The solid curves correspond to the best fits of the experimental data below CMC by the theoretical model, described in Section 3.1. The dashed lines represent the plateau above the CMC.

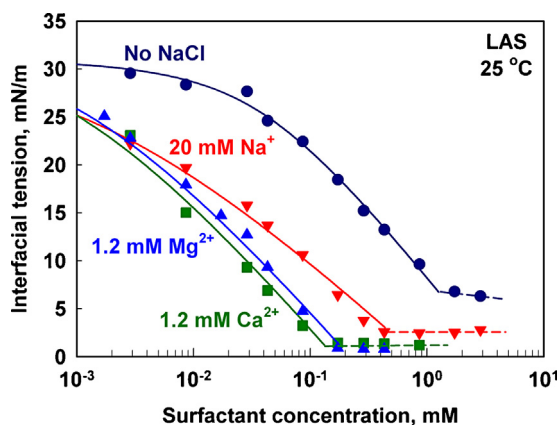
does not exceed 0.85 at the CMC for any of the salt concentrations studied. This result shows that the adsorption layer is not fully saturated, even at the onset of micelle formation, which is in agreement with the results reported by Thomas et al. [28,29].

Fig. S2 depicts the evaluated occupancy of the Stern layer  $\theta_{\text{Na}}$  with bound  $\text{Na}^+$  counter-ions. We see that the adsorption layer is almost completely depleted of  $\text{Na}^+$  ions, in the presence of 1.2 mM  $\text{Ca}^{2+}$  or  $\text{Mg}^{2+}$  in the solution. In contrast, the occupancy  $\theta_{\text{Na}}$  rises up to approximately 0.45 in the absence of hardness ions ( $\text{Ca}^{2+}$  or

$\text{Mg}^{2+}$ ) which corresponds to 55% ionization of LAS headgroups in the adsorption layer.

The dependence of  $\theta_{\text{Ca}}$  on surfactant concentration is illustrated in Fig. S3. In this case,  $\text{Ca}^{2+}$  occupies up to ca. 45% of the Stern layer at the CMC, which refers to only 10% ionization of the surfactant adsorption layer, because  $\theta_{\text{Ca}} = 0.5$  concurs to completely neutralized Stern layer ( $\text{Ca}^{2+}$  is a divalent cation).

The plot of  $\Phi_s$  vs. surfactant concentration is shown in Fig. 5. Interestingly, in the absence of added electrolyte, the surface potential passes through a maximum. The latter observation can be attributed to the competition of two opposite trends [21]: (i) the



**Fig. 2.** LAS adsorption isotherms on SBO–water interface in presence of  $\text{Na}^+$ ,  $\text{Mg}^{2+}$  and  $\text{Ca}^{2+}$  ions. The solid curves correspond to the best fits of the experimental data below CMC by the theoretical model, presented in Section 3.1. The dashed lines represent the plateau above the CMC. Circles correspond to surfactant without added electrolyte, down triangles stand for 20 mM NaCl, up triangles correspond to 1.2 mM  $\text{MgCl}_2$ , and squares stand for 1.2 mM  $\text{CaCl}_2$ .

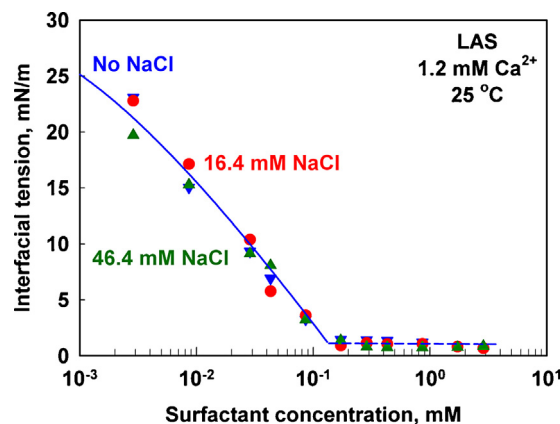


**Fig. 3.** LAS adsorption isotherms on SBO–water interface in presence of 1.2 mM  $\text{Ca}^{2+}$  and various ionic strengths (3.6 mM – down triangles, 20 mM – circles and 50 mM – up triangles). The solid curve corresponds to the best fit of the experimental data below the CMC by the theoretical model, described in Section 3.1. The dashed line represents the plateau above the CMC.

**Table 1**

Adsorption parameters ( $\alpha_\infty$  and  $\Delta\mu_1^0$ ) for LAS on oil–water and air–water interfaces, in the presence of various inorganic salts. The binding energies of the counter-ions are  $\Delta\mu_2^0 = 0 kT$  and  $\Delta\mu_4^0 = 3.5 kT$ .

LAS	Oil–water		Air–water	
	$\alpha_\infty$ (nm <sup>2</sup> )	$\Delta\mu_1^0$ (kT)	$\alpha_\infty$ (nm <sup>2</sup> )	$\Delta\mu_1^0$ (kT)
No salt	1.06 ± 0.17	20.0 ± 0.5	0.83 ± 0.13	21.1 ± 0.5
+Na <sup>+</sup>	0.73 ± 0.12	17.8 ± 0.4	0.52 ± 0.09	18.9 ± 0.5
+Mg <sup>2+</sup>	0.56 ± 0.09	16.0 ± 0.4	0.35 ± 0.06	16.3 ± 0.4
+Ca <sup>2+</sup>	0.55 ± 0.09	16.2 ± 0.4	0.29 ± 0.05	16.3 ± 0.4

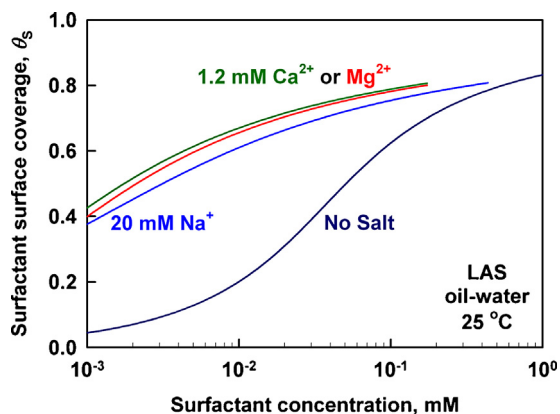


**Fig. 4.** Surface coverage,  $\theta_s$ , vs. surfactant concentration for various salt concentrations. The solid curves represent numerical results of the theoretical model after interpreting the experimental data for the respective interfacial tensions.

surface electric charge rises with surfactant adsorption and (ii) the counter-ions dissociated from the ionic surfactant bind in the Stern layer. When salt is added to the surfactant solution, the counter-ion concentration in the bulk is almost constant and effect (ii) is less significant.

**Fig. 5** also demonstrates that the addition of 1.2 mM Mg<sup>2+</sup> or Ca<sup>2+</sup> to the solution reduces significantly  $\Phi_s$  – the surface electrostatic potential in presence of 1.2 mM Ca<sup>2+</sup> is approximately –56 mV. On the other hand, Na<sup>+</sup> ions are not so effective in lowering the surface electric potential, which is –126 mV in presence of 20 mM NaCl. These differences are related to the stronger attraction of the divalent cations to the negatively charged interfacial layer.

Next, we calculated the surface coverage  $\theta_s$  and the dimensionless surface potential  $\Phi_s$  as a function of salt concentration, see Figs. S4 and S5. From Fig. S4 one can compare the effects of Na<sup>+</sup> and Ca<sup>2+</sup> on surfactant adsorption. In the case of 0.01 mM LAS, even

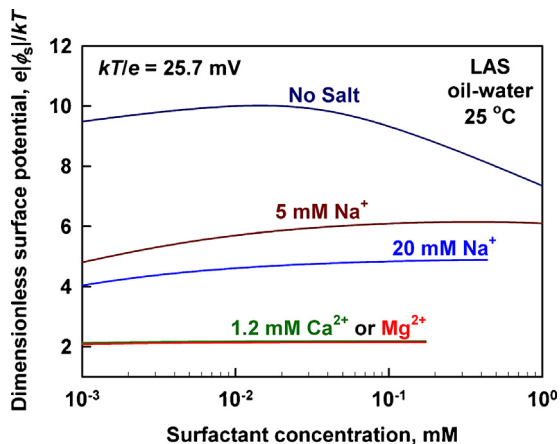


**Fig. 5.** Dimensionless surface potential,  $\Phi_s$ , as a function of surfactant concentration for various salt concentrations. The solid curves represent numerical results of the theoretical model.

a small concentration of salt is sufficient to change strongly the saturation of the adsorption layer, viz. from 0.2 to 0.7. It is intriguing that 1.2 mM Ca<sup>2+</sup> produces the same or even greater effect in terms of surface coverage, compared to 50 mM NaCl. Only 0.03 mM Ca<sup>2+</sup> in 0.01 mM LAS solution is sufficient to increase the surfactant adsorption significantly, viz.  $\theta_s$  rises from 0.2 to 0.5.

**Figure S5** clearly shows that the addition of merely 0.03 mM Ca<sup>2+</sup> lowers  $\Phi_s$  from 9.7 (= –250 mV) to 3.9 (= –100 mV) which illustrates the fact that the strong binding of Ca<sup>2+</sup> leads to suppressed electrostatic repulsion between the adsorbed surfactant molecules. Na<sup>+</sup> ions also suppress electrostatic repulsion, but much more inefficiently compared to hardness ions.

### 5.3. Comparison of LAS adsorption on oil–water and air–water interfaces

To compare the LAS adsorption on oil–water and air–water interfaces we used Wilhelmy plate method to determine the equilibrium surface tension and to construct the adsorption isotherms of LAS on air–water interface, at different salt concentrations.

The obtained surface tension isotherms are compared in **Fig. 6** with the respective interfacial tension isotherms, in terms of the respective surface pressures,  $\pi(c_{1\infty})$ . One sees that the slope  $d\pi/d\ln c_{1\infty}$ , roughly proportional to the surfactant adsorption density, is up to  $\approx 50\%$  higher for air–water interface, compared to oil–water interface. In other words,  $\Gamma_1$  is much greater for air–water interface than for oil–water interface. Quantitative comparison could be made by considering the excluded areas per LAS molecule for both types of interfaces which are also shown in the respective graph (**Figs. 6A–D**). These areas were calculated using the theoretical model described in Section 3. One sees that LAS forms more compact adsorption layer on air–water interface, compared to oil–water interface. In the absence of salt (**Fig. 6A**) the respective areas are 0.83 nm<sup>2</sup> vs. 1.06 nm<sup>2</sup>. Even bigger is the difference in the presence of electrolytes, especially in the presence of divalent counter-ions – the areas per molecule are almost two times larger for oil–water interface (0.29 nm<sup>2</sup> vs. 0.55 nm<sup>2</sup>). This difference has to be explained with the intercalation of oil molecules between the surfactant molecules in the adsorption layer, as the other possible mechanism (dissolution of the surfactant into the oily phase) is not relevant to LAS, because this is an ionic surfactant without nonionic contaminations (the latter would lead to minimum in the surface tension isotherms).

For both interfaces, hardness ions effectively screen the electrostatic repulsion of LAS headgroups, thus leading to better packing of the molecules on the interface: the excluded area per molecule decreases approximately two times in the presence of Mg<sup>2+</sup> or Ca<sup>2+</sup>, compared to the salt free case. This remarkable reduction of the area per molecule is expected to be related to structural rearrangement of the LAS molecules in the adsorption layer, when Ca<sup>2+</sup> or Mg<sup>2+</sup> are present in the solution.

For the sake of completeness, in **Fig. 7** we compare also the surfactant surface coverage  $\theta_s$  and the dimensionless surface potential  $\Phi_s$  in the presence and in the absence of 1.2 mM Ca<sup>2+</sup>. The data demonstrate that both  $\theta_s$  and  $\Phi_s$  do not differ significantly for air–water and oil–water interfaces. This is to be expected, as  $\theta_s$  is the ratio of  $\Gamma_1$  to  $\Gamma_\infty$ , which change almost proportionately; and  $\Phi_s$  depends primarily on the binding energies of the counter-ions which are similar for A/W and O/W interfaces.

### 5.4. Adsorption parameters for LAS on oil–water and air–water interfaces

The adsorption parameters determined from the best fit to the experimental data, are shown in **Table 1**. As mentioned above, the theoretical fit was not very sensitive to the ratios  $K_2/K_1$  and  $K_4/K_1$

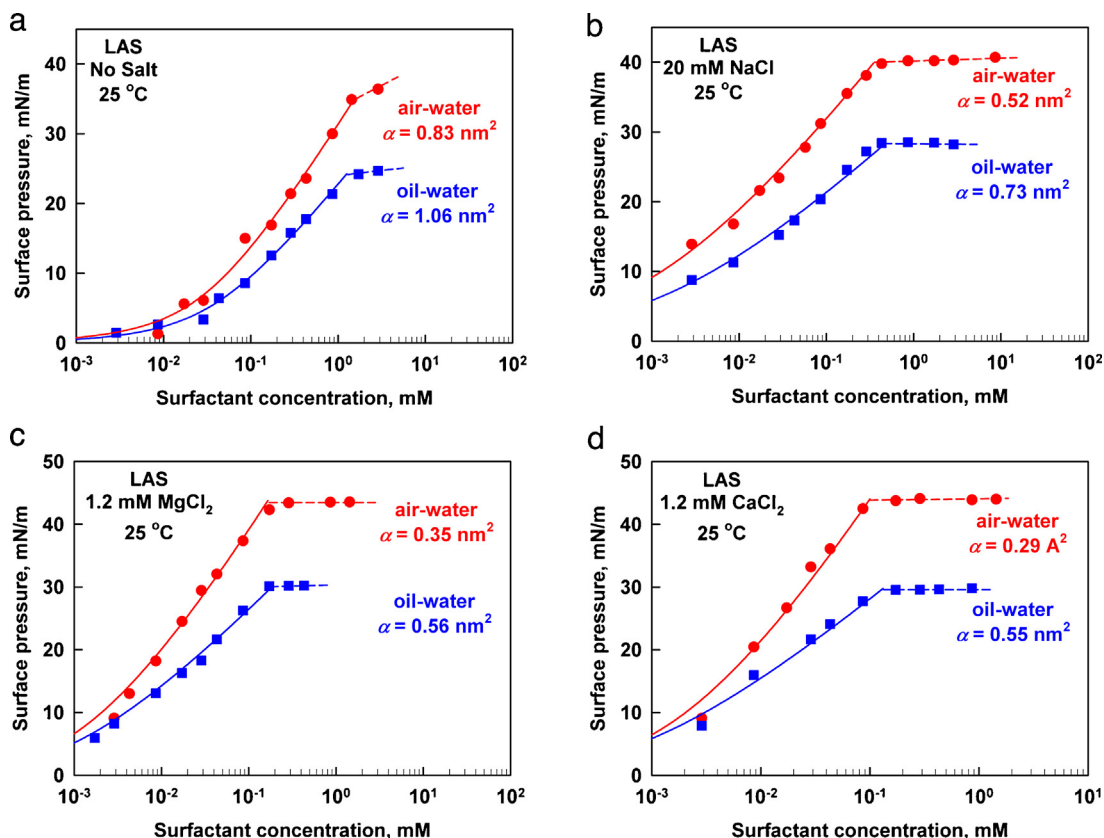


**Fig. 6.** Comparison of surface and interfacial tension isotherms for the following cases: (A) no added salt, (B) 20 mM NaCl, (C) 1.2 mM MgCl<sub>2</sub> and (D) 1.2 mM CaCl<sub>2</sub>. By  $\alpha$  we denote the excluded area per molecule. The solid curves correspond to the best fits of the experimental data below CMC, by the theoretical model described in Section 3.1. The dashed lines represent the plateau above the CMC.

(related to the values of  $\Delta\mu_2^0$  and  $\Delta\mu_4^0$ , respectively), i.e. the merit function goes through a shallow minimum when varying these ratios. Therefore, we fixed the non-electrostatic binding energies of the counter-ions as follows: (i)  $\Delta\mu_2^0 = 0 \text{ kT}$  for Na<sup>+</sup>, and (ii)  $\Delta\mu_4^0 = 3.5 \text{ kT}$  for Mg<sup>2+</sup> and Ca<sup>2+</sup>. These specific values were chosen on the basis of the electrophoretic mobility measurements of the oil drops, as explained in Section 5.5. On the other hand, the values of  $\alpha_\infty$  and  $\Delta\mu_1^0$  are estimated in a reliable way, with very small relative errors, see Fig. S6.

Our results for the excluded area per LAS molecule at the air–water interface were compared with reference data from other authors. Meader and Criddle [1] determined that  $\alpha_\infty$  varies from

0.33 up to 1.12 nm<sup>2</sup>, depending on the specific positional isomer of LAS used. The largest area is occupied by the isomer, in which the hydrophilic group is in the center of the dodecyl hydrocarbon chain [1,2,30]. This range of values is similar to the values determined in our study.

By applying Gibbs adsorption equation, Ma et al. [2] deduced the area per molecule at CMC,  $\alpha_{\text{CMC}} = 1/\Gamma_{\text{CMC}}$ , from surface tension measurements. They found that  $\alpha_{\text{CMC}}$  falls in the range between 0.43 and 0.65 nm<sup>2</sup>, which are smaller values compared to our result ( $\alpha_{\text{CMC}} \approx 1 \text{ nm}^2$ ) in the absence of added inorganic salts. Using neutron reflectivity (NR), Tucker and co-workers [3,4] determined a limiting area (corresponding to  $\alpha_{\text{CMC}}$ ) per LAS molecule for the

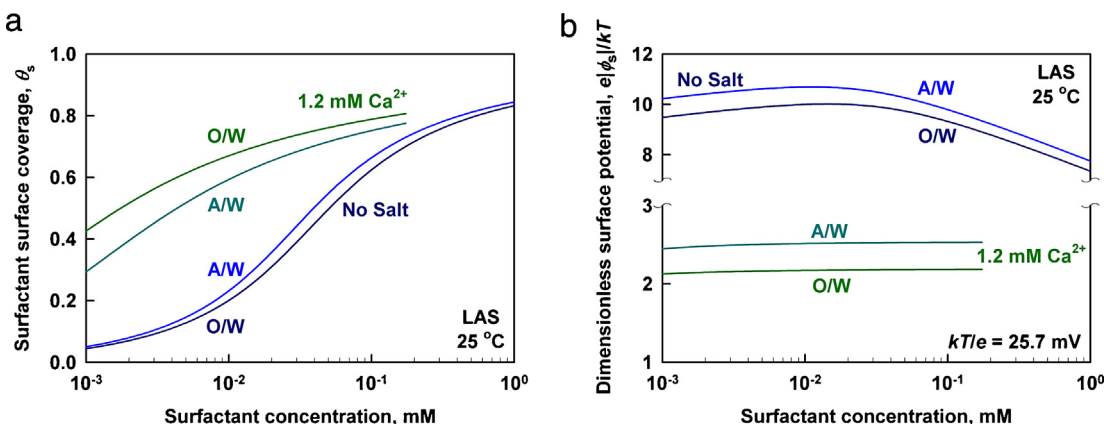


**Fig. 7.** Comparison of LAS properties on air–water and oil–water interfaces in the presence and in the absence of 1.2 mM Ca<sup>2+</sup>: (A)  $\theta_s(c_{1\infty})$  and (B)  $\Phi_s(c_{1\infty})$ . The solid curves are numerical results of the theoretical model.

symmetric LAS6 isomer (positional isomer of LAS, for which the benzene ring is attached at the sixth carbon atom of the alkyl chain) of  $\approx 0.57 \text{ nm}^2$ , again significantly smaller value than our  $\alpha_{\text{CMC}}$  of  $1 \text{ nm}^2$ . To explain this discrepancy, we compared our surface tension data with the data of Ma et al., see Fig. S7. One sees in Fig. S7 a pronounced difference in the slope  $d\sigma/d\ln c$  for the two studies, which must be due to different composition of the LAS samples used. We characterized LAS sample by high-performance liquid chromatography (HPLC); see Fig. S8. The HPLC chromatogram shows that our technical grade LAS contains isomers with tails ranging from C10 to C13 and the fine structure of each peak corresponds to the respective positional isomer of LAS. By conductivity measurements we found that our LAS sample contains ca. 4.5 wt%  $\text{Na}_2\text{SO}_4$ . However, the numerical calculations showed that the presence of  $\text{Na}_2\text{SO}_4$  cannot explain the observed differences between the various studies.

The main trends, however, are very similar for all studies performed with LAS. For example, the values for  $\alpha_\infty$  show that hardness ions considerably compact the LAS adsorption layer on both types of interfaces, air–water and oil–water. Indeed,  $\text{Mg}^{2+}$  and  $\text{Ca}^{2+}$  reduce the area per LAS molecule on oil–water interface from  $1.06 \text{ nm}^2$  to  $0.55 \text{ nm}^2$ . Such compaction or even multilayer formation has been observed at the air–water interface for LAS in presence of  $\text{Ca}^{2+}$  [3,4]. The monovalent  $\text{Na}^+$  has similar, but much smaller effect on LAS adsorption behavior.

Concerning the standard free energy of surfactant adsorption  $\Delta\mu_1^0$ , we notice that it varies in the range from about 16–21  $kT$ . The main contribution to  $\Delta\mu_1^0$  is coming from the energy for transfer of the surfactant tail from bulk water to the interface. According to Traube's rule, the transfer of one methylene group ( $\text{CH}_2$ ) from the water to the air costs 1.025  $kT$ . Since the tail of LAS consists of a dodecyl chain and a benzene ring, the energy for tail transfer is at least 12.3  $kT$ ; the energy for transfer of the benzene ring on the phase boundary is unknown, however, it should be on the order of several  $kT$  units. On the other hand, we observe that  $\Delta\mu_1^0$  decreases as the area per molecule  $\alpha_\infty$  becomes smaller. The latter result might be explained as follows: upon addition of counter-ions, the adsorption layer undergoes structural changes which affect the head-group contribution to  $\Delta\mu_1^0$  which is usually proportional to  $\alpha_\infty$  (it corresponds to the disappearance of bare air–water or oil–water interface upon surfactant adsorption).

To estimate the accuracy of the adjustable parameters ( $\alpha_\infty$  and  $\Delta\mu_1^0$ ), we studied the merit function  $\chi$  in the vicinity of its

minimum. In Fig. S6, we present the analysis for LAS+ $\text{Ca}^{2+}$  on oil–water interface, as a two-dimensional contour plot. We also estimated the confidence intervals for  $\alpha_\infty$  and  $\Delta\mu_1^0$ , for which the interval boundaries correspond to  $1.25\chi_{\text{min}}$ . The data are presented in Table 1: the relative errors of  $\alpha_\infty$  and  $\Delta\mu_1^0$  are 16% and 2.5%, respectively, which shows that these parameters are determined with reasonably high accuracy.

### 5.5. Estimation of $\Phi_s$ from zeta potential measurements with oil drops.

We performed electrophoretic measurements of diluted oil-in-water emulsions in order to estimate the surface electric potential of LAS interfacial layer, in presence of electrolytes. For more information about the way of data interpretation from these measurements, see Appendix A.

As  $\Phi_s$  is rather sensitive to the binding energies of the counter-ions, we could check experimentally whether  $\Delta\mu_2^0$  and  $\Delta\mu_4^0$  are determined accurately. The experimental and theoretical results deduced from the zeta potential measurements are summarized in Table 2. The values of  $\Phi_s$ , determined from the electrophoretic measurements, are compared to the numerical values obtained from the theoretical interpretation of the interfacial tension data, see Sections 3 and 4. As seen from the last three columns of Table 2, the agreement for  $\text{Ca}^{2+}$  and  $\text{Mg}^{2+}$  is remarkably good. For instance, we calculate from both types of experiments  $\Phi_s \approx 2.5$  for 0.6 mM  $\text{Ca}^{2+}$  and  $\Phi_s \approx 2.2$  for 1.2 mM  $\text{Ca}^{2+}$ , with very weak dependence on surfactant concentration.

In contrast, the zeta potentials measured in the presence of hardness ions decrease with the increase of surfactant concentration. A possible explanation of this trend could be a slight shift in the position of the shear plane at higher surfactant concentrations, which results in a reduced absolute value of the measured  $\zeta$ -potential [31]. As seen in Table 2, the deduced dimensionless surface potentials from the electrophoretic experiments for these solutions fall in interval between 2 and 3, as predicted from the interfacial tension data interpretation. For  $\text{Na}^+$  we see that  $\Phi_s$  from the theoretical model also agrees with the results from the electrophoretic experiments. This agreement of the two sets of data for  $\Phi_s$ , determined by two independent methods, supports strongly the reliability of the values of the ionic binding constants and of the surface potentials, as determined from the interfacial tension measurements.

**Table 2**

Zeta potentials and surface potentials of oil droplets, formed in LAS solution with added inorganic salt. The surface potential,  $\Phi_s$ , is estimated in two ways: (i) by applying Eq. (A.8) for two distances  $\delta$  between the Stern layer and the shear plane, and (ii) from the fits of the interfacial tension data by the theoretical model in Section 3.

$c(\text{LAS})$ (mM)	$c(\text{NaCl})$ (mM)	$\zeta$ (mV)	$-e\zeta/kT$	$\Phi_s$ (from Eq. (A.8))		$\Phi_s$ (from $\sigma$ vs. $c$ )
				$\delta = 0.28 \text{ nm}$	$\delta = 0.56 \text{ nm}$	
0.01	5	$-113 \pm 3$	4.40	5.09	6.15	5.70
0.1		$-130 \pm 2$	5.06	6.12	8.53	6.09
$c(\text{LAS})$ (mM)	$c(\text{CaCl}_2)$ (mM)	$\zeta$ (mV)	$-e\zeta/kT$	$\Phi_s$ (from Eq. (A.8))		$\Phi_s$ (from $\sigma$ vs. $c$ )
				$\delta = 0.28 \text{ nm}$	$\delta = 0.56 \text{ nm}$	
0.01	0.6	$-58.8 \pm 2.0$	2.29	2.54	2.87	2.51
0.1		$-48.3 \pm 0.6$	1.88	2.04	2.22	2.53
0.01	1.2	$-57.5 \pm 0.7$	2.24	2.59	3.14	2.17
0.1		$-49.3 \pm 0.5$	1.92	2.16	2.48	2.18
$c(\text{LAS})$ (mM)	$c(\text{MgCl}_2)$ (mM)	$\zeta$ (mV)	$-e\zeta/kT$	$\Phi_s$ (from Eq. (A.8))		$\Phi_s$ (from $\sigma$ vs. $c$ )
				$\delta = 0.28 \text{ nm}$	$\delta = 0.56 \text{ nm}$	
0.01	0.6	$-59.8 \pm 1.0$	2.33	2.59	2.94	2.48
0.1		$-49.3 \pm 2.0$	1.92	2.08	2.28	2.49
0.01	1.2	$-60.8 \pm 0.2$	2.37	2.78	3.49	2.14
0.1		$-51.2 \pm 1.1$	1.99	2.25	2.61	2.15

## 6. Summary and conclusions

The experimental data show that  $\text{Mg}^{2+}$  and  $\text{Ca}^{2+}$  ions markedly reduce the interfacial tension  $\sigma$  and the CMC of LAS solutions: the effect of 1.2 mM  $\text{Mg}^{2+}$  or  $\text{Ca}^{2+}$  is much more significant than that of 20 mM NaCl. The reason for this strong effect of  $\text{Mg}^{2+}$  or  $\text{Ca}^{2+}$  ions is that these ions bind much more strongly to the surfactant headgroups than the monovalent  $\text{Na}^+$  cations, thus suppressing the electrostatic repulsion for surfactant adsorption or monomer incorporation in the micelles.

Interestingly, when 1.2 mM  $\text{Ca}^{2+}$  is present in the surfactant solution, the interfacial tension  $\sigma$  depends very slightly on NaCl concentration which demonstrates that  $\text{Na}^+$  ions cannot replace  $\text{Ca}^{2+}$  ions in the Stern layer. A possible explanation is provided by the data interpretation in Section 5. We demonstrate that the interaction of  $\text{Na}^+$  with LAS is purely electrostatic ( $\Delta\mu_2^0 \approx 0$  kT), whereas both  $\text{Mg}^{2+}$  and  $\text{Ca}^{2+}$  have very high specific binding energies ( $\Delta\mu_4^0 \approx 3.5$  kT) besides the stronger electrostatic binding, typical for the divalent counter-ions. The higher affinity of hardness ions to LAS headgroups (both electrostatic and specific) leads to almost exhaustive condensation of these ions in the Stern layer; hence, the surface charge and potential are strongly reduced and so is the electrostatic barrier for surfactant adsorption.

We compared LAS adsorption on air–water (A/W) and oil–water (O/W) interfaces in presence of various counter-ions. In the absence of salt, we determined an excluded area per LAS molecule of  $\alpha_\infty = 0.83$  nm<sup>2</sup> on A/W interface and  $\alpha_\infty = 1.06$  nm<sup>2</sup> on O/W interface. The larger area on O/W interface can be explained by intercalation of oil molecules in between the surfactant molecules in the adsorption layer.

Remarkable is the fact that even a minor amount of  $\text{Mg}^{2+}$  or  $\text{Ca}^{2+}$  leads to almost twice more compact adsorption layer on both A/W and O/W interfaces. The respective areas per molecule are:  $\alpha_\infty = 0.29$  nm<sup>2</sup> on A/W interface and  $\alpha_\infty = 0.55$  nm<sup>2</sup> on O/W interface. This strong reduction of the limiting area per molecule indicates a significant restructuring in the packing of the LAS molecules in the presence of  $\text{Mg}^{2+}$  or  $\text{Ca}^{2+}$  ions.

To validate the theoretical predictions of the model, we conducted electrophoretic experiments with oil droplets which showed that the surface potentials, determined from the adsorption isotherms, agree fairly well with those extracted from zeta potential measurements (especially in the presence of divalent counter-ions). The latter agreement is a strong support for the reliability of the obtained adsorption parameters from the interfacial tension data.

## Acknowledgements

We thankfully acknowledge the support from Unilever Research Centre, Bangalore, India; Unilever R&D, Port Sunlight, UK (PS-2012-1190); and the FP7 project Beyond-Everest (FP7-REGPOT-2011-1). The authors are grateful to Mrs. Mila I. Temelska for some of the interfacial tension measurements and to Mrs. Zlatina G. Mitrinova for the HPLC analysis – both from Sofia University.

## Appendix A. Surface potential of oil droplets

Our goal here is to estimate the surface potential of oil droplets from zeta potential measurements in the presence of divalent counter-ions. Neglecting any curvature effects, we start with the relationship between the electric potential  $\varphi$  and the bulk charge density  $\rho_b$ , given by the Poisson equation for flat interface, which reads:

$$\frac{d^2\varphi}{dx^2} = -\frac{\rho_b}{\varepsilon\varepsilon_0}, \quad (\text{A.1})$$

where  $\varepsilon\varepsilon_0$  is the dielectric permittivity of the medium (in our case water). Assuming that the ions in the solution obey Boltzmann distribution, Eq. (A.1) is transformed into the Poisson–Boltzmann equation:

$$\frac{d^2\Phi}{dx^2} = \kappa_c^2 [c_{2\infty} \sinh \Phi + c_{4\infty} (\exp(2\Phi) - \exp(-\Phi))], \quad (\text{A.2})$$

where  $\Phi \equiv -e\varphi/kT$  is the dimensionless electric potential.

If we multiply both sides of Eq. (A.2) by  $2d\Phi/dx$  and then integrate, the following expression is obtained:

$$\begin{aligned} \left(\frac{d\Phi}{dx}\right)^2 &= 2\kappa_c^2 \left[ c_{2\infty} (\cosh \Phi - 1) + \frac{c_{4\infty}}{2} (\exp(2\Phi) - 1) + c_{4\infty} (\exp(-\Phi) - 1) \right], \end{aligned} \quad (\text{A.3})$$

where we imposed that both  $\Phi$  and  $d\Phi/dx$  vanish at infinity. Taking into account that  $\Phi$  is a decreasing function of distance,  $x$ , the square root of Eq. (A.3) yields:

$$\frac{d\Phi}{dx} = -\kappa_c \sqrt{I_1} \frac{y^2 - 1}{y} g_1, \quad (\text{A.4})$$

where

$$\begin{aligned} I_1 &\equiv c_{2\infty} + 3c_{4\infty}, \quad \lambda^2 \equiv \frac{c_{4\infty}}{I_1}, \quad y = \exp\left(\frac{\Phi}{2}\right), \\ g_1 &= (1 - \lambda^2 + \lambda^2 y^2)^{1/2}. \end{aligned} \quad (\text{A.5})$$

By integrating Eq. (A.4) we obtain an expression for the distance  $\delta$  between the Stern layer and the shear plane:

$$\delta = \frac{2}{\kappa_c \sqrt{I_1}} \int_{y_{sh}}^{y_s} \frac{dy}{(y^2 - 1)g_1}, \quad (\text{A.6})$$

where

$$y_s = \exp\left(\frac{\Phi_s}{2}\right), \quad y_{sh} = \exp\left(\frac{-e\zeta}{2kT}\right). \quad (\text{A.7})$$

The integral in Eq. (A.6) can be solved analytically and its solution is as follows:

$$\begin{aligned} \delta &= \frac{1}{\kappa_c \sqrt{I_1}} [d(y_s) - d(y_{sh})], \\ d(y) &= \ln \left| \frac{(y-1)[\lambda^2(y+1) - 1 - g_1]}{(y+1)[\lambda^2(y-1) + 1 + g_1]} \right|. \end{aligned} \quad (\text{A.8})$$

We could estimate  $\Phi_s$  by solving Eq. (A.8) numerically, assuming that the shear plane is shifted at a distance of one or two water molecules away from the Stern layer (the diameter of a water molecule is 0.28 nm [24]) and the oil droplet  $\zeta$ -potential is taken from the electrophoretic experiments.

## Appendix B. Supplementary data

Supplementary data associated with this article can be found, in the online version, at <http://dx.doi.org/10.1016/j.colsurfa.2014.10.059>.

## References

- [1] A.L. Meader Jr., D.W. Criddle, Force-area curves of surface films of soluble surface-active agents, *J. Colloid Sci.* 8 (1953) 170.
- [2] J.-G. Ma, B.J. Boyd, C.J. Drummond, Positional isomers of linear sodium dodecyl benzene sulfonate: solubility, self-assembly, and air/water interfacial activity, *Langmuir* 22 (2006) 8646.

- [3] I. Tucker, J. Penfold, R.K. Thomas, C.C. Dong, S. Golding, C. Gibson, I. Grillo, Surface and solution properties of anionic/nonionic surfactant mixtures of alkylbenzene sulfonate and triethyleneglycol decyl ether, *Langmuir* 26 (2010) 10614.
- [4] I. Tucker, J. Penfold, R.K. Thomas, C.C. Dong, S. Golding, C. Gibson, I. Grillo, The adsorption and self-assembly of mixtures of alkylbenzene sulfonate isomers and the role of divalent electrolyte, *Langmuir* 27 (2011) 6674.
- [5] Y. Li, X.J. He, W.L. Cao, G.Q. Zhao, X.X. Tian, X.H. Cui, Molecular behavior and synergistic effects between sodium dodecylbenzene sulfonate and Triton X-100 at oil/water interface, *J. Colloid Interface Sci.* 307 (2007) 215.
- [6] N.M. van Os, L.A.M. Rupert, B. Smit, P.A.J. Hilbers, K. Esselink, M.R. Bohmer, L.K. Koopal, Surfactant adsorption at liquid/liquid interfaces. Comparison of experimental results with self-consistent field lattice calculations and molecular dynamics simulations, *Colloids Surf. A* 81 (1993) 217.
- [7] D.B. Ludlum, Micelle formation in solutions of some isomeric detergents, *J. Phys. Chem.* 60 (1956) 1240.
- [8] N.M. van Os, G.J. Daane, T.A.B.M. Bolsman, The effect of chemical structure upon the thermodynamics of micellization of model alkylarenesulfonates: II. Sodium p-(3-alkyl)benzenesulfonate homologs, *J. Colloid Interface Sci.* 123 (1988) 267.
- [9] A. Sein, J.B.F.N. Engberts, Micelle to lamellar aggregate transition of an anionic surfactant in dilute aqueous solution induced by alkali metal chloride and tetraalkyl-ammonium chloride salts, *Langmuir* 11 (1995) 455.
- [10] C.L. McFearin, D.K. Beaman, F.G. Moore, G.L. Richmond, From Franklin to today: toward a molecular level understanding of bonding and adsorption at the oil–water interface, *J. Phys. Chem. C* 113 (2009) 1171.
- [11] J.C. Conboy, J.L. Daschbach, G.L. Richmond, Studies of alkane/water interfaces by total internal reflection second harmonic generation, *J. Phys. Chem.* 98 (1994) 9688.
- [12] R.M.A. Azzam, N.M. Bashara, *Ellipsometry and Polarised Light*, North-Holland Publishing Co., 1977.
- [13] S.C. Russev, T.V. Arguirov, T.D. Gurkov, Beta-casein adsorption kinetics on air–water and oil–water interfaces studied by ellipsometry, *Colloids Surf. B* 19 (2000) 89.
- [14] L.T. Lee, D. Langevin, B. Farnoux, Neutron reflectivity of an oil–water interface, *Phys. Rev. Lett.* 67 (1991) 2678.
- [15] K. Golemanov, S. Tcholakova, N. Denkov, E. Pelan, S.D. Stoyanov, The role of the hydrophobic phase in the unique rheological properties of saponin adsorption layers, *Soft Matter* 10 (2014) 7034.
- [16] A.G. Gaonkar, R.P. Borwankar, Adsorption behavior of monoglycerides at the vegetable oil/water interface, *J. Colloid Interface Sci.* 146 (1991) 525.
- [17] A.G. Gaonkar, R.P. Borwankar, Competitive adsorption of monoglycerides and lecithin at the vegetable oil–water interface, *Colloids Surf.* 59 (1991) 331.
- [18] T.D. Gurkov, D.T. Dimitrova, K.G. Marinova, C. Bilke-Crause, C. Gerber, I.B. Ivanov, Ionic surfactants on fluid interfaces: determination of the adsorption; role of the salt and the type of the hydrophobic phase, *Colloids Surf. A* 261 (2005) 29.
- [19] S.S. Dukhin, G. Kretzschmar, R. Miller, *Dynamics of Adsorption at Liquid Interfaces*, Elsevier, Amsterdam, 1995.
- [20] A.W. Adamson, A.W. Gast, *Physical Chemistry of Surfaces*, sixth ed., Wiley, New York, 1997.
- [21] P.A. Kralchevsky, K.D. Danov, G. Broze, A. Mehreteab, Thermodynamics of ionic surfactant adsorption with account for the counterion binding: effect of salts of various valency, *Langmuir* 15 (1999) 2351.
- [22] V.L. Kolev, K.D. Danov, P.A. Kralchevsky, G. Broze, A. Mehreteab, Comparison of the van der Waals and Frumkin adsorption isotherms for sodium dodecyl sulfate at various salt concentrations, *Langmuir* 18 (2002) 9106.
- [23] S. Chanda, D. Das, J. Das, K. Ismail, Adsorption characteristics of sodium dodecyl-sulfate and cetylpyridinium chloride at air/water, air/formamide and air/water–formamide interfaces, *Colloids Surf. A* 399 (2012) 56.
- [24] J.N. Israelachvili, *Intermolecular and Surface Forces*, third ed., Academic Press, Amsterdam, 2011.
- [25] I.B. Ivanov, K.D. Danov, D. Dimitrova, M.I. Boyanov, K.P. Ananthapadmanabhan, A. Lips, Equations of state and adsorption isotherms of low molecular non-ionic surfactants, *Colloids Surf. A* 354 (2010) 118.
- [26] M.L. Corrin, W.D. Harkins, The effect of salts on the critical concentration for the formation of micelles in colloidal electrolytes, *J. Am. Chem. Soc.* 69 (1947) 683.
- [27] J. Penfold, E. Staples, I. Tucker, R.K. Thomas, Surface ordering in dilute dihexadecyl dimethyl ammonium bromide solutions at the air–water interface, *Langmuir* 20 (2004) 2265.
- [28] J.R. Lu, A. Marrocco, T.J. Su, R.K. Thomas, J. Penfold, Adsorption of dodecyl sulfate surfactants with monovalent metal counterions at the air–water interface studied by neutron reflection and surface tension, *J. Colloid Interface Sci.* 158 (1993) 303.
- [29] J.R. Lu, I.P. Purcell, E.M. Lee, E.A. Simister, R.K. Thomas, A.R. Rennie, J. Penfold, The composition and structure of sodium dodecyl sulfate–dodecanol mixtures adsorbed at the air–water interface: a neutron reflection study, *J. Colloid Interface Sci.* 174 (1995) 441.
- [30] S. Das, R.G. Bhirud, N. Nayyar, K.S. Narayan, V.V. Kumar, Chemical shift changes on micellization of linear alkyl benzenesulfonate and oleate, *J. Phys. Chem.* 96 (1992) 7454.
- [31] P.A. Kralchevsky, K.D. Danov, N.D. Denkov, Chemical physics of colloid systems and interfaces, in: K.S. Birdi (Ed.), *Handbook of Surface and Colloid Chemistry*, CRC Press LLS, Boca Raton, 1997 (Chapter 11).